Cardiovascular Research (2011) **92**, 57–66
doi:10.1093/cvr/cvr180

NCX is an important determinant for premature ventricular activity in a drug-induced model of Andersen–Tawil syndrome

Przemysław B. Radwański[1,2] and Steven Poelzing[1,3]*

[1]Nora Eccles Harrison Cardiovascular Research and Training Institute, University of Utah, 95 South 2000 East, Salt Lake City, UT 84112-5000, USA; [2]Department of Pharmacology and Toxicology, University of Utah, 95 South 2000 East, Salt Lake City, UT 84112-5000, USA; and [3]Department of Bioengineering, University of Utah, 95 South 2000 East, Salt Lake City, UT 84112-5000, USA

Received 21 January 2011; revised 8 June 2011; accepted 15 June 2011; online publish-ahead-of-print 21 June 2011

Time for primary review: 21 days

Aims Andersen–Tawil syndrome (ATS1)-associated ventricular arrhythmias are initiated by premature ventricular activity (PVA) resulting from diastolic Ca^{2+} (Ca_D) accumulation. We hypothesized that relatively high Na^+–Ca^{2+} exchanger (NCX) expression coupled with slower Ca^{2+} uptake may constitute an arrhythmogenic substrate during drug-induced ATS1 (DI-ATS1).

Methods and results DI-ATS1 was induced with 10 μmol/L $BaCl_2$ and 2 mmol/L $[K^+]_o$. Ca^{2+} transients and action potentials were optically mapped from Langendorff-perfused guinea pig ventricles. Intracellular Ca^{2+} handling was modulated by either direct NCX inhibition with 5 μmol/L KB-R7943 or by sarcoplasmic reticulum Ca^{2+}-ATPase (SERCA2a) inhibition with cyclopiazonic acid (CPA). During DI-ATS1, PVA was more frequent in left ventricular (LV)-base (LVB) vs. LV-apex (LVA) (2.2 ± 0.8 vs. 0.6 ± 0.3 PVA/10 min), consistent with greater Ca_D (1.65 ± 0.13 vs. 1.42 ± 0.09 normalized-Ca_D units) and western blot-assessed NCX protein expression (81.2 ± 30.9%) in LVB relative to LVA. Further, regions of high NCX (LVB) evidenced a shorter PVA coupling interval relative to regions of low NCX expression (LVA, 67.7 ± 3.5 vs. 78.5 ± 3.6%). Inhibiting NCX during DI-ATS1 lowered the incidence of ventricular tachycardias (VTs, 0 vs. 25%) and PVA (1.5 ± 0.4 vs. 4.3 ± 1.4 PVA/10 min), but it did not affect PVA coupling intervals in LVB nor LVA (70.8 ± 4.3 vs. 73.8 ± 2.5%). Conversely, inhibition of SERCA2a with CPA, thereby increasing the role of NCX in Ca^{2+} handling, significantly increased the incidence of VTs and PVA relative to DI-ATS1 alone, while decreasing the PVA coupling interval in all regions.

Conclusion PVA preferentially occurs in regions of enhanced NCX expression with relatively slower Ca^{2+} uptake and during perfusion of CPA which further reduces sarcoplasmic reticular Ca^{2+} uptake.

Keywords Arrhythmia • Calcium • Ventricular arrhythmias

1. Introduction

Anderson–Tawil syndrome (ATS1) is an autosomal dominant inherited channelopathy linked to a loss-of-function mutation in *KCNJ2*, the gene that encodes the Kir2.1 channel which is responsible for carrying the inward-rectifier K^+ current.[1] ATS1 is characterized by a mild QT prolongation and ventricular arrhythmias that are initiated by frequent, hypokalaemia-exacerbated, premature ventricular activity (PVA).[1] These triggered events have been linked to abnormal Ca^{2+} regulation,[2] particularly elevated diastolic cytosolic Ca^{2+} levels (Ca_D) and presumed sarcoplasmic reticulum (SR) Ca^{2+} overload.[1] However, the relationship between regional perturbation in Ca^{2+} cycling and the origin of PVA from a specific site is not clear.

More specifically, PVA which has been demonstrated to originate from areas of elevated Ca_D, was caused by membrane depolarization in response to non-electrically induced Ca^{2+} release from the SR.[3] Briefly, it is thought that spontaneous SR Ca^{2+} release occurs secondarily to elevated Ca_D which may increase the probability for the specialized SR release channels, ryanodine receptors, to release Ca^{2+}.[3] Similarly, the combination of elevated Ca_D and enhanced SR Ca^{2+} entry via SR Ca^{2+}-ATPase (SERCA2a) may overload the SR with Ca^{2+}, further increasing the probability for a spontaneous

* Corresponding author. Tel: +1 801 585 1862; fax: +1 801 581 3128. Email: poelzing@cvrti.utah.edu

Ca^{2+} release.[4,5] Regardless of the mechanism leading to spontaneous Ca^{2+} release, the non-electrogenic release of Ca^{2+} from the SR requires the Na^{+}–Ca^{2+} exchanger (NCX) operating in its forward mode (3 Na^{+}-in–Ca^{2+}-out) to cause a rise in membrane potential and thereby a propagated beat.

Previous work using ventricular tissue has suggested that regions with lowest SERCA2a expression, thereby the regions with the weakest ability to overload the SR, experience the greatest propensity for PVA.[6] Therefore, we hypothesize that in our drug-induced model of ATS1 (DI-ATS1), regions of higher NCX functional expression and weaker SERCA2a may serve as a potential substrate for arrhythmias. We propose that Ca_D by itself is not the putative marker for PVA. Conversely, we demonstrate that it is heterogeneous Ca^{2+} cycling that correlates with incidence of PVA and arrhythmias. Specifically, regions with enhanced cytosolic Ca^{2+} accumulation coupled to relatively higher NCX functional expression and weaker SERCA2a exhibits closer coupled and more frequent premature activity.

2. Methods

This investigation conforms with the Guide for the Care and Use of Laboratory Animals published by the US National Institutes of Health (NIH Publication No. 85-23, revised 1996) and has been approved by the Institutional Animal Care and Use Committee of the University of Utah (protocol no. 05-07002).

2.1 Experimental preparation

Retired-breeder guinea pigs ($n = 44$) were anaesthetized by an overdose of sodium pentobarbital (30 mg/kg). Deep anaesthesia was confirmed by lack of response to noxious stimuli. Hearts were rapidly excised and Langendorff-perfused with 36.5°C oxygenated Tyrode's solution containing (mmol/L) $CaCl_2$ 2, NaCl 140, KCl 4.5, dextrose 10, $MgCl_2$ 1, and HEPES 10 (pH 7.41). They were stained with either the voltage-sensitive dye di-4-ANEPPS (15 μmol/L) or Indo-1/AM (1 μmol/L) by direct coronary perfusion. ATS1 was modelled as described previously by perfusion of 10 μmol/L $BaCl_2$ and hypokalaemic (2 mmol/L KCl) Tyrode's solution.[7] Motion was reduced using 7.5 mmol/L 2,3-diacetylmonoxime. Ventricles were stimulated from the septum at 1.5 times the stimulation threshold with bipolar stainless steal electrodes at a basic cycle length of 400 ms. Volume-conducted electrocardiograms (ECGs) were continuously recorded to assess arrhythmia burden. In a subset of ventricles ($n = 3$), we inserted an intramural multielectrode needle into the basal left ventricle (LVB) to assess transmural activation patterns.

2.2 Experimental interventions

NCX dominance was altered by pharmacologically inhibiting either NCX or SERCA2a with KB-R7943 or cyclopiazonic acid (CPA), respectively. In isolated guinea pig atria, 10–30 μM KB-R7943 suppressed ouabain-induced arrhythmias;[8] however, in isolated rat cardiomyocytes, Satoh *et al.*[9] demonstrated that 5 μM KB-R7943 did not effect twitch contractions or Ca^{2+} transients but reduced spontaneous activity during sodium loading. Therefore, in order to study the role of NCX in DI-ATS1-associated arrhythmias, we used 5 μM KB-R7943.

On the other hand, SERCA2a function in guinea pig cardiomyocytes was completely inhibited by both thapsigargin and high doses of CPA;[10] therefore, in our study just as in Szentesi *et al.*, doses in the lower range of CPA (5 μmol/L) were used. This allowed us to achieve partial SERCA2a blockade as evidenced in our study by a 25–30% prolongation in Ca^{2+} transient decay constant (τ) during CPA perfusion.

2.3 Optical voltage and Ca^{2+} mapping

Optical voltage and Ca^{2+} mapping was used as previously described using the ratiometric fluorescence method.[7] Specifically, we used two SciMedia MiCam02 HS CCD cameras (SciMedia) in a tandem lens configuration with 1 ms temporal resolution from 90 × 60 sites simultaneously. For voltage recordings, the preparation was excited by three 60-LED light sources (RL5-A9018, Superbrightleds). The resultant fluorescence was filtered by either 610 nm LP filter (Newport) or 540 ± 10 nm filter (Chroma) before it was incident on the CCD array. The relative change in voltage was determined by dividing the fluorescence at 610 nm by the fluorescence at 540 nm. On the other hand, for Ca^{2+} mapping, we first recorded at both emission wavelengths (485 and 405 nm) the background fluorescence representing tissue autofluorescence. Excitation light was obtained from a 1000 W mercury arc lamp (Thermo-Oriel) and filtered at 350 ± 10 nm (Chroma). After indo-1 staining, the resultant fluorescence was passed through emission filters (either 485 ± 10 or 405 ± 10 nm) and incident on CCD arrays. Ratiometric measurements of Ca^{2+} transients were determined by dividing the background-subtracted fluorescence Ca^{2+} transients at 405 nm by the background-subtracted fluorescence Ca^{2+} transients at 485 nm.

2.4 Western blotting

Western immunoblotting for NCX and SERCA2a was performed as described previously.[11] Briefly, four parts of the anterior ventricular free walls were snap-frozen and homogenized. Samples with equal amounts of protein, as assessed by BCA assay, were resolved by SDS–polyacrylamide electrophoresis on 4–12% Bis–Tris gels (BioRad, Hercules, CA, USA). The proteins were then transferred onto a nitrocellulose membrane. After blocking non-specific binding of antibodies with 5% casein solution, the membrane was treated with primary antibody [mouse monoclonal anti-SERCA2a/anti-NCX1 monoclonal antibody/anti-actin antibody (Affinity BioReagents, Golden, CO, USA)] followed by goat anti-mouse HRP-conjugated secondary antibody (JacksonImmuno, West Grove, PA, USA). The membrane was then treated with enzymatic chemiluminescence reagents, and the bands were visualized on autoradiography film.

Protein expression in the samples was quantified on the basis of the size and density of the bands. SERCA2a and NCX expression levels were normalized to the regional actin expression for inter-animal comparison.

2.5 Data analysis

Activation time was defined as the time of the maximum first derivative of the action potential as described previously.[7] Repolarization was defined as the time to 95% repolarization from peak voltage amplitude. Action potential duration (APD) was the time difference between activation and full repolarization. APD dispersion was defined as the difference between epicardial regions with the longest and shortest APD (using 25 spatially contiguous optically mapped sites per region). PVA coupling interval was the per cent of the PVA interval and the average beat-to-beat interval of five preceding beats. Excitation times from the intramural multielectrode needle were the time of maximum negative QRS slope in the unipolar

electrgorams.[12] Relative Ca_D level was defined as the minimum ratiometric signal before the Ca^{2+} transient upstroke. In order to compare relative changes between different experiments, the offset of Ca_D was drift corrected as described previously.[7] Regional Ca_D levels were normalized to the apical right ventricular (RV) Ca_D level obtained during the initial recording (i.e. control or DI-ATS1). The rate of cytosolic Ca^{2+} decay to diastolic levels (30–100% of the decline phase) was fit to a single exponential (τ).[6] Statistical analysis was performed with a two-tailed Student's *t*-test or a single factor ANOVA with *post hoc* Student's *t*-tests for continuous, normally distributed paired data, with statistical significance assumed for values of $P < 0.05$, with correction for multiple comparisons (Sidak adjusted) where necessary. A Fisher's exact and a Mantel–Haenszel test were used to test differences in nominal data. Differences in PVA frequency were analysed using Wilcoxon's signed-rank test for non-normally distributed continuous data. All statistical comparisons were made on paired data. All values are reported as means ± standard error unless otherwise noted.

3. Results

3.1 Heterogeneous manifestations of PVA

Figure 1A (top) depicts ECGs of intrinsic beats from three bath leads. The isochrone map of the resulting epicardial activation (*Figure 1A*, bottom) reveals two characteristic anterior epicardial breakthrough sites, one on each ventricle. In the case of a representative PVA, the QRS complex was discordant relative to those of the preceding intrinsic beats in all three ECG leads (*Figure 1B*, top), and the earliest epicardial activation occurred in the LVB (*Figure 1B*, bottom). Similarly, concordant PVA depicted on the ECGs (*Figure 1C*, top) evidenced earliest epicardial activation in LV-apex (LVA; *Figure 1C*, bottom). Activation arising from the anterior RV and indeterminate areas as quantified by optical mapping exhibited QRS morphologies different from the prior two cases (data not shown).

Regional PVA frequency was quantified from ECGs collected over the duration of the experiment, and QRS orientation in three leads (all leads concordant or discordant) was used as an index of the PVA origination site. Over 90% of PVA during DI-ATS1 originated from the LV (either the LVB or the LVA). PVA originating from other sites (*Figure 1D*) occurred with lower frequency relative to LV PVA (0.1 ± 0.1 vs. 2.8 ± 0.6 PVA/10 min). Among LV PVA, significantly more originated from the LVB relative to the LVA (2.2 ± 0.8 vs. 0.6 ± 0.3 PVA/10 min; *Figure 1D*). Further, optically mapped activity revealed that LVB PVA was more closely coupled to the preceding intrinsic beat than LVA PVA (67.7 ± 4.7 vs. 78.5 ± 3.6%; *Figure 1E*); however, this difference was not noted when comparing all PVA recorded on volume-conducted ECGs (70.8 ± 1.8 vs. 70.7 ± 1.9%; *Figure 1F*). Lastly, the mean QRS duration of intrinsic beats was significantly shorter than all PVA (*Figure 1G*). Additionally, QRS duration of LVB PVA was significantly longer relative to LVA PVA (49.3 ± 1 vs. 44.6 ± 1.4 ms; *Figure 1G*). QRS orientation and duration in the bath leads were used to quantify the PVA origination site.

3.2 Multifocal origins of PVA

Examining the transmural activation of the intrinsic beat during DI-ATS1 by intramural multielectrode needle electrograms revealed sequential transmural activation starting with the endocardium, which then spread to the mid-myocardium and subsequently to the epicardium (*Figure 1H*). In the case of one LVB PVA (*Figure 1I*), the layer of earliest transmural activation corresponded to the epicardium. While in another example of LVB PVA (*Figure 1J*), the layer of earliest transmural activation corresponded to the endocardium.

3.3 Spatiotemporal correlation of heterogeneous cytosolic Ca^{2+} levels and PVA

Representative control Ca^{2+} transients (*Figure 2A*, grey traces) demonstrate higher Ca_D in the LV relative to the RV. Over all experiments, control Ca_D was significantly higher in the LVB relative to RVA (*Figure 2B*, grey bars). During DI-ATS1, Ca_D increased in all regions (*Figure 2A*, black traces) but retained its LV to RV gradient. Importantly, the LVB exhibited the highest Ca_D levels during DI-ATS1 (black bars) relative to other anterior epicardial regions (*Figure 2B*).

3.4 Ca^{2+} transient decay

Comparing representative normalized Ca^{2+} transients (from 0 to 1; *Figure 2C*), there were no quantifiable differences in the duration or the decay kinetics of the Ca^{2+} transients between control (grey traces) and DI-ATS1 (black traces). Ca^{2+} transients in LVA decayed faster than LVB (*Figure 2D*, inset) or RV regions (*Figure 2C*). However, Ca^{2+} transient decay time constants (τ) were not different between control and DI-ATS1 in any region (*Figure 2D*). Further, LVA evidenced significantly shorter τ relative to LVB by 10.1 ± 2.1 ms (*Figure 2D*), as well as RV regions under all conditions.

3.5 SERCA2a protein expression

SERCA2a expression was quantified by western blotting using homogenized tissue samples from the guinea pig. Actin was used to normalize for differences in lane loading. Representative bands in *Figure 3A* corresponding to SERCA2a (outlined in blue) and actin (outlined in black) demonstrate greater SERCA2a band density in LVA relative to LVB. Indeed, over all experiments, actin-normalized SERCA2a expression was significantly greater in the LVA compared with the LVB by 76.8 ± 23.6% (*Figure 3B*), which is consistent with faster Ca^{2+} transient decay kinetics in the LVA and slower Ca^{2+} transient decay kinetics throughout the remainder of the myocardium (*Figure 2C* and *D*).

3.6 NCX protein expression

NCX was also quantified by western blotting as described above. Representative bands in *Figure 3C* corresponding to NCX (outlined in red) and actin (outlined in black) demonstrate greater NCX expression in LVB relative to LVA. Over all experiments, actin-normalized NCX expression was significantly greater in the LVB compared with the LVA by 81.2 ± 30.9% (*Figure 3D*), but no significant differences in NCX expression were noted within the RV.

3.7 Pharmacological SERCA2a inhibition

SERCA2a inhibition with CPA during DI-ATS1 resulted in a global Ca_D level elevation by 21.1 ± 2.6% (*Figure 4A*; see Supplementary material online, *Figure S1A*). All values in *Figure 4A* were normalized to DI-ATS1 in the RVA. Further, SERCA2a inhibition slowed Ca^{2+} transient decay only in the LV (raw traces in Supplementary material online, *Figure S1B*). In summary, CPA increased τ in LVB and LVA by 17.0 ± 5.2 and 10.9 ± 2.7 ms, respectively (*Figure 4B*).

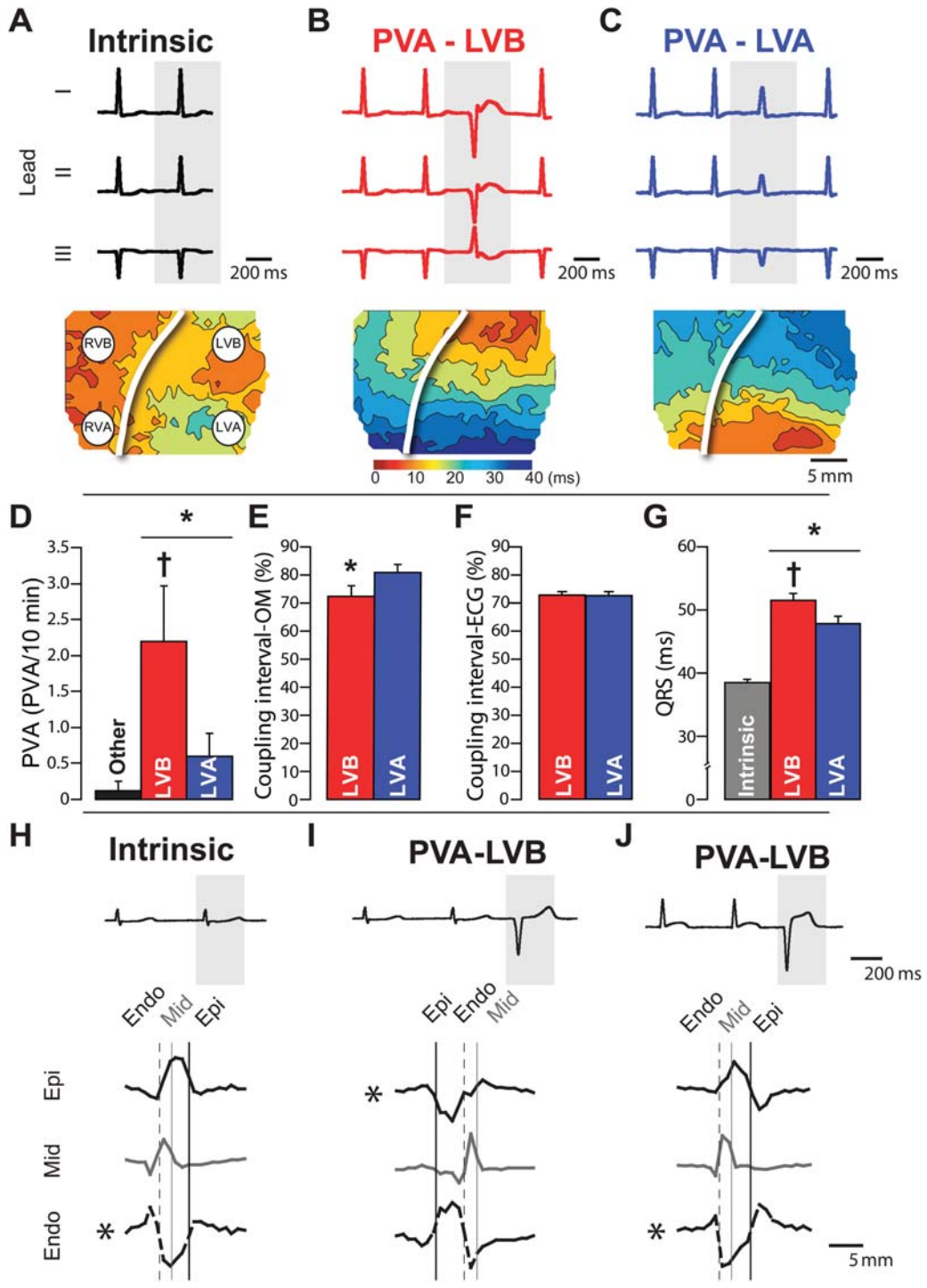

Figure 1 During DI-ATS1, PVA originates preferentially from LVB and is multifocal in nature. (*A*) Representative volume-conducted ECGs of intrinsic beats during DI-ATS1 (top) and resulting activation isochrone map (bottom). (*B*) Discordant PVA on volume-conducted ECGs (red ECGs, top) evidenced earliest anterior epicardial activation in the LVB (bottom). (*C*) PVA with concordant QRS morphology (blue ECGs, top) originated in LVA (bottom). (*D*) PVA originating from other sites (RV and indeterminate areas) occurred less frequently relative to LV PVA ($^{*}P < 0.05$, $n = 10$), while those originating from LVB occurred more frequently relative to LVA PVA ($^{\dagger}P < 0.05$). (*E*) Optically mapped LVB PVA were more closely coupled to the preceding intrinsic beat than LVA PVA ($^{*}P < 0.05$, $n = 7$). (*F*) No differences in coupling interval were noted when PVA quantified from volume-conducted ECGs ($n = 10$). (*G*) The mean QRS duration of intrinsic beats was narrower relative to all types of PVA ($^{*}P < 0.05$, $n = 10$), while QRS duration of LVB PVA was wider relative to LVA PVA ($^{\dagger}P < 0.05$, $n = 10$). (*H*) Representative volume-conducted ECG of intrinsic beats recorded during DI-ATS1 (top) and corresponding intramural multielectrode needle electrograms (bottom) revealing sequential activation of the intrinsic beat starting with the endocardium (Endo, *), proceeding through the mid-myocardium (Mid), and lastly activating epicardium (Epi). (*I*) Representative PVA consistent with LVB activation (top) reveals epicardial (Epi, *) origin of the ectopy (bottom), while (*J*) another representative LVB PVA (top) reveals endocardial (Endo, *) origin of ectopy (bottom).

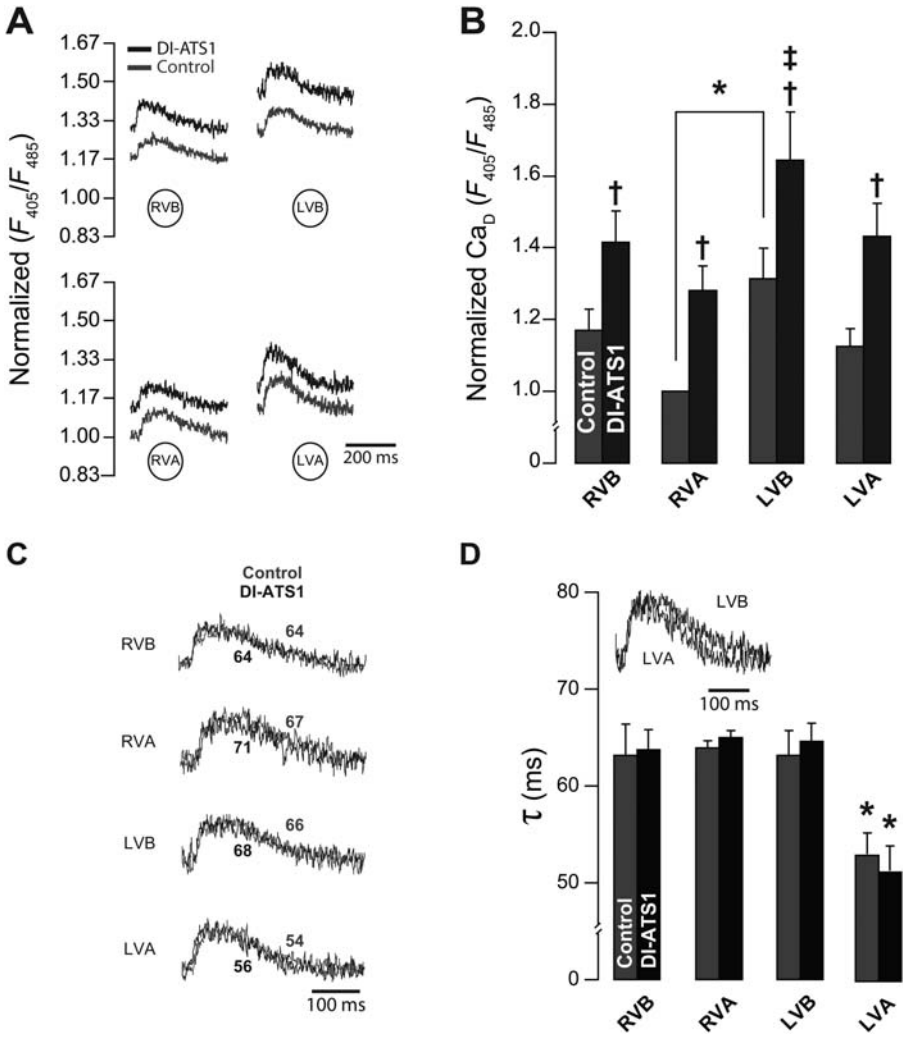

Figure 2 Cytosolic Ca^{2+} levels and Ca^{2+} transient decay kinetics during DI-ATS1. (*A*) Representative Ca^{2+} transients recorded from same ventricular regions demonstrate higher Ca_D in LV relative to RV during control (grey traces) and an upward Ca_D shift in all regions during DI-ATS1 (black traces). (*B*) The mean RVA normalized Ca_D during control was greater in LVB relative to RVA ($^*P < 0.05$, $n = 8$). During DI-ATS1, Ca_D increased in all regions ($^{\dagger}P < 0.05$, $n = 8$). LVB exhibited highest Ca_D levels relative to other anterior epicardial regions ($^{\ddagger}P < 0.05$). (*C*) Representative normalized Ca^{2+} transients (from 0 to 1) (same as above) demonstrate high degree of morphological correspondence and no quantifiable difference in Ca^{2+} transient decay constant (τ) within regions between control (grey traces) and DI-ATS1 (black traces). However, LVA Ca^{2+} transients decay faster relative to RV and (*D*) LVB (inset). (*D*) The mean τ was not different between control and DI-ATS1 in any region. LVA evidenced shorter τ relative to LVB as well as RV regions ($^*P < 0.05$, $n = 5$).

3.8 Pharmacological NCX inhibition

Conversely, NCX inhibition by KB-R7943 during DI-ATS1 significantly increased Ca_D in both LVB and LVA by 14.1 ± 3.0 and 13.5 ± 3.0%, respectively (*Figure 4C*). There was no measurable effect of NCX blockade on Ca^{2+} transient decay kinetics as demonstrated in Supplementary material online, *Figure S1D*. Overall, NCX inhibition did not significantly affect τ (*Figure 4D*). However, the LVA still maintained the fastest Ca^{2+} uptake kinetics (shortest τ) relative to all other regions.

3.9 SERCA2a inhibition and arrhythmias

Enhancing the role of NCX in Ca^{2+} handling during DI-ATS1 by SERCA2a inhibition (DI-ATS1 + CPA) increased the incidence of spontaneous ventricular tachycardias (VTs) three-fold relative to DI-ATS1 (58.3 vs. 16.7% of preparations, respectively, *Figure 5A*), as well as the frequency of PVA from both LVB and LVA (*Figure 5B*) without effecting the incidence of other regional PVA. Yet, the difference in PVA frequency between the LVB and LVA was no longer statistically significant during DI-ATS1 + CPA. Lastly, CPA decreased PVA coupling interval relative to DI-ATS1 alone (*Figure 5C*).

3.10 NCX inhibition and arrhythmias

Conversely, NCX inhibition with KB-R7943 during DI-ATS1 (DI-ATS1 + KB-R7943) reduced incidence of spontaneous VTs to zero (0 of 8 hearts) from 25% (2 of 8) during DI-ATS1 (*Figure 5D*; $P = 0.11$). DI-ATS1 + KB-R7943 also lowered the frequency of LVB PVA (*Figure 5E*), but not LVA (*Figure 5E*) or the other regional PVA. Further, NCX inhibition during DI-ATS1 did not alter the coupling

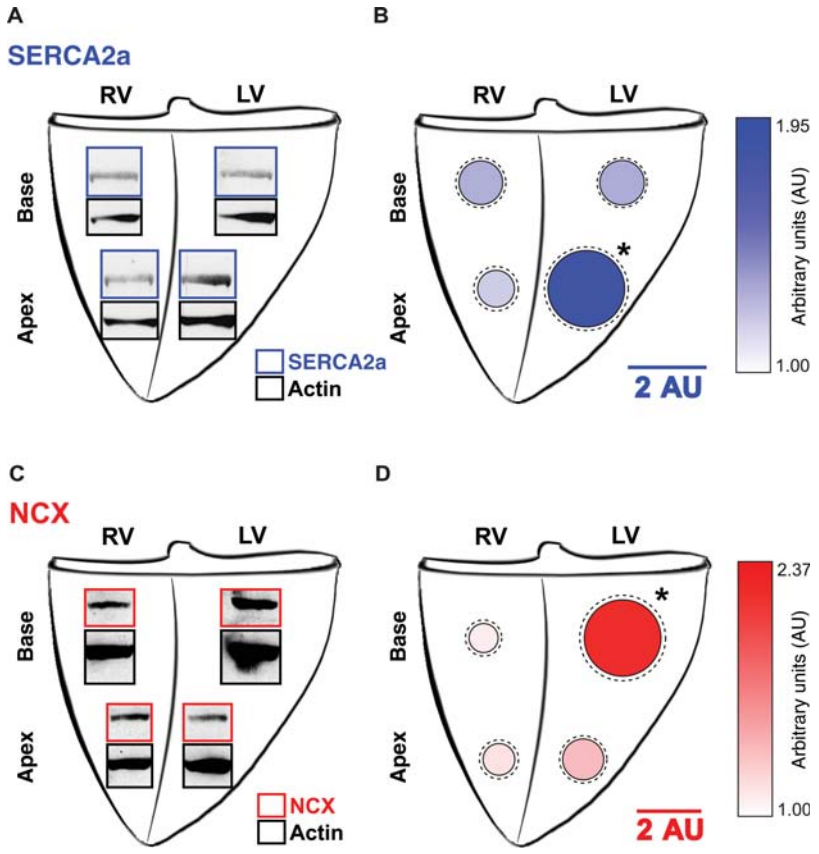

Figure 3 NCX dominance spatially correlates with PVA. (*A*) Representative SERCA2a bands (blue outline) and actin bands (black outline) from different anterior epicardial regions. (*B*) Actin-normalized SERCA2a protein expression in each region is denoted by the radius and colour of the corresponding circle, while dashed circles reflect standard error. The mean actin-normalized SERCA2a protein expression in LVA was 76.8 ± 23.6% greater than in LVB (*$P < 0.05$, $n = 6$), whereas no significant difference was observed within RV (P = NS). (*C*) Representative NCX (red outline) and actin (black outline) demonstrate greater NCX band density in LVB relative to LVA. (*D*) The mean actin-normalized NCX expression was significantly greater in LVA by 81.2 ± 30.9% compared with the LVB (*$P < 0.05$, $n = 5$).

interval of PVA quantified from continuous ECG recordings relative to DI-ATS1 alone (*Figure 5F*).

3.11 Action potential duration

Representative action potentials in *Figure 6A* during control (grey traces) demonstrate existing APD heterogeneities between RVB and LVA (previously demonstrated to have the longest and shortest APDs, respectively).[7,13] DI-ATS1 (*Figure 6A*, black traces) prolonged APD globally, preserving aforementioned APD heterogeneities between RVB and LVA (*Figure 6C*, black traces). SERCA2a inhibition (*Figure 6A*, red traces) prolonged APD in both RVB and LVA relative to DI-ATS1 alone (*Figure 6A*, black traces); however, to a lesser extent when compared with NCX inhibition (*Figure 6D*). Indeed, over all experiments, DI-ATS1 + CPA prolonged APD in LVA significantly more than in RVB relative to DI-ATS1 alone by 15.8 ± 2.1 vs. 9.5 ± 2.7%, respectively (*Figure 6B*), which significantly reduced APD dispersion (*Figure 6C*). Conversely, NCX blockade during DI-ATS1 (*Figure 6D*, blue traces) prolonged APD and maintained APD dispersion relative to DI-ATS1 alone. Over all experiments, APD was prolonged by 32.1 ± 2.2% in RVB and 34.2 ± 3.0% in LVA during DI-ATS1 + KB-R7943 relative to DI-ATS1 alone (*Figure 6E*), resulting in a persistently elevated APD dispersion (*Figure 6F*) relative to control.

4. Discussion

In this study, we investigated the factors underlying the arrhythmogenic burden during cytosolic Ca^{2+} overload in DI-ATS1.[2,7] We found that APD and APD dispersion did not correlate with arrhythmias observed during DI-ATS1. The preponderance of PVA originated from regions of relatively high Ca_D and NCX protein expression. However, pharmacological inhibition of SERCA2a increased while inhibition of NCX decreased PVA. Therefore, data presented herein suggest that increased PVA is dependent on a specific combination of relatively high Ca_D accumulation and high NCX.

4.1 APD and arrhythmias

Dispersion of repolarization is an important substrate for the genesis of reentrant ventricular arrhythmias associated with some long QT syndromes.[14] During DI-ATS1, APD, APD dispersion, and arrhythmic burden were increased relative to control, consistent with previous reports.[2,7]

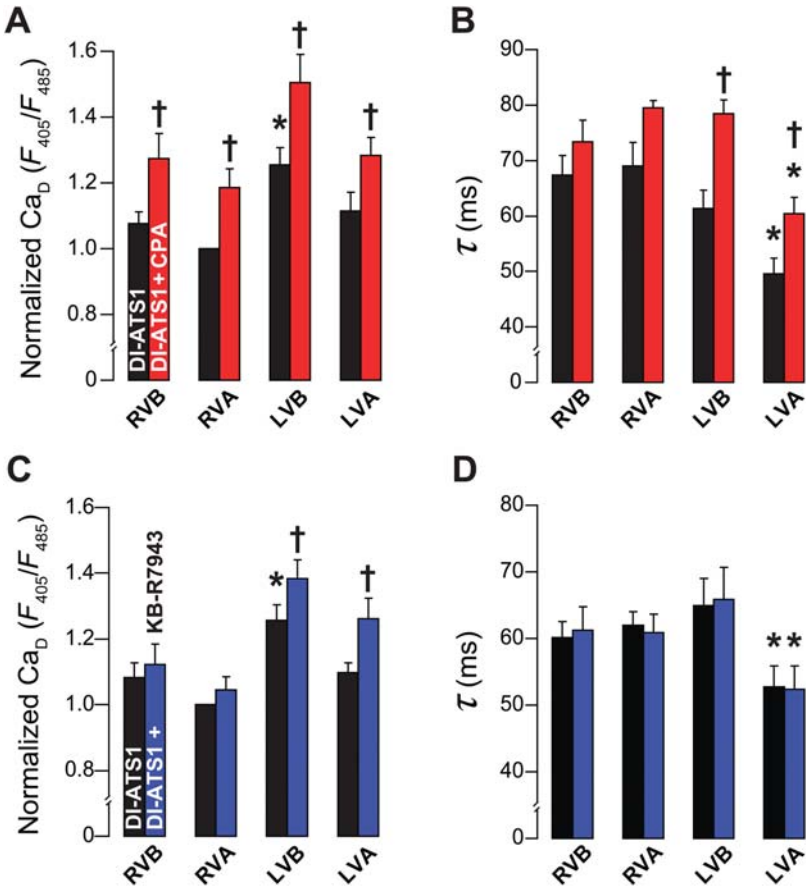

Figure 4 SERCA2a but not NCX inhibition prolongs Ca^{2+} transient decay kinetics. (*A*) The mean Ca_D during DI-ATS1 was higher in the LVB relative to RVA (*$P < 0.05$, $n = 6$), while SERCA2a inhibition by CPA during DI-ATS1 (DI-ATS1 + CPA) increased Ca_D globally ($^{\dagger}P < 0.05$). (*B*) The mean Ca^{2+} transient decay constant (τ) was lowest in the LVA during DI-ATS1 and DI-ATS1 + CPA (*$P < 0.05$, $n = 4$) despite mean τ prolongation in the LV by DI-ATS1 + CPA ($^{\dagger}P < 0.05$). (*C*) NCX inhibition by KB-R7943 during DI-ATS1 (DI-ATS1 + KB-R7943, blue bars) resulted in mean Ca_D rise only in the LV ($^{\dagger}P < 0.05$, $n = 5$). (*D*) The mean τ demonstrate similar τ between DI-ATS1 and DI-ATS1 + KB-R7943, where LVA evidenced lowest τ relative to other anterior epicardial regions (*$P < 0.05$, $n = 5$).

SERCA2a inhibition with CPA during DI-ATS1 prolonged APD, decreased APD dispersion, and significantly increased arrhythmias. The observed increase in APD with CPA (5 μmol/L) is consistent with previous reports in the hamster papillary muscle.[15]

NCX inhibition during DI-ATS1 increased APD, maintained APD dispersion observed during DI-ATS1 alone, and, yet, decreased arrhythmias. Taken together, these data suggest that APD prolongation and dispersion are an unlikely substrate for reentrant arrhythmias during DI-ATS1.

4.2 Regional manifestations of PVA during DI-ATS1

The higher preponderance of PVA originating from the LVB in this study is consistent with the PVA origination site in a rat heart model of oxidative stress,[16] as well as a rabbit model of hypokalaemia[17] and long QT Type 2.[18] Furthermore, Fujiwara *et al.* demonstrated that the PVA originating from LVB was virtually abolished by NCX inhibition,[17] consistent with our results. Epicardial mapping cannot determine the transmural origins of PVA. We, therefore, provide evidence that PVA occurred from different transmural depths as measured with needle electrodes. This is consistent with results from Morita *et al.*[2] who demonstrated under similar DI-ATS1 experimental conditions multifocal transmural PVA in a canine LV wedge preparation. Therefore, the remainder of this study focused on elucidating protein correlates of higher LVB arrhythmic burden, without regard to transmural layers.

4.3 Sarcoplasmic reticulum Ca^{2+}-ATPase and premature ventricular activity

It was previously proposed that elevated Ca^3_D and subsequent SR Ca^{2+} load[19] can precipitate PVA.[4] In the guinea pig, regions of high SERCA2a coupled to ubiquitous phospholamban expression (Supplementary material online, *Figure S2*) did not correlated with increased PVA. Pharmacologically inhibiting SERCA2a with CPA slowed the decay kinetics of the Ca^{2+} transient and further increased Ca_D consistent with previous results.[20] Importantly, CPA increased PVA, decreased PVA coupling interval, and increased Ca_D. In isolated guinea pig cardiomyocytes, Szentesi *et al.*[10] demonstrated that a comparable dose of CPA reduced SR Ca^{2+} content by 50%. Plainly speaking, tissue with the weakest ability to load the SR is most susceptible

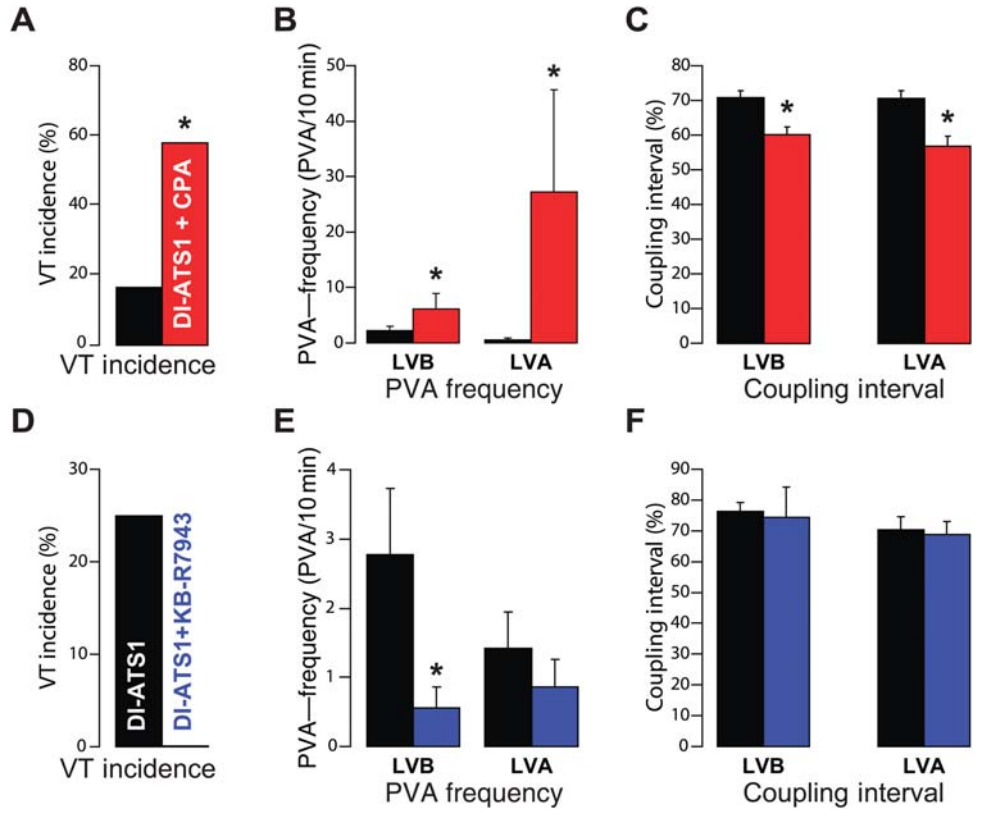

Figure 5 NCX dominance underlies arrhythmias during DI-ATS1. (*A*) SERCA2a inhibition during DI-ATS1 (DI-ATS1 + CPA) increased incidence of spontaneous VT relative to DI-ATS1 alone (7 vs. 2, $n = 12$, respectively, $^*P < 0.05$). (*B*) PVA frequency, defined as the number of events per 10 min, was increased both in the LVB and LVA during DI-ATS1 + CPA compared with DI-ATS1 alone ($^*P < 0.05$, $n = 10$). (*C*) DI-ATS1 + CPA shortened the mean coupling interval of PVA to the preceding intrinsic beat both for LVB and LVA PVA ($^*P < 0.05$, $n = 10$). (*D*) Conversely, out of eight preparations tested, spontaneous VTs were observed in two (25%) preparations during DI-ATS1 and none during concomitant NCX inhibition and DI-ATS1 (DI-ATS1 + KB-R7943, $P = 0.11$). (*E*) Over all PVA, frequency originating from LVB was decreased during DI-ATS1 + KB-R7943 relative to DI-ATS1 alone ($^*P < 0.05$, $n = 8$). (*F*) The mean coupling interval of PVA to the preceding intrinsic beat was unaltered in either LV region by DI-ATS1 + KB-R7943 ($P =$ NS, $n = 8$).

to the earliest and most frequent PVA in this model. Thus, these data suggest that low SERCA2a expression is related to increased Ca_D as previously demonstrated,[6,21] but SR Ca^{2+} overload may not be the underlying mechanism of PVA in DI-ATS1.[6] These data do not preclude that elevated Ca_D alone increases the probability of SR Ca^{2+} releases as has been suggested previously.[3]

4.4 NCX and premature ventricular activity

In contrast, regions with relatively high NCX protein expression exhibited high PVA during DI-ATS1. Further, pharmacologically inhibiting NCX with KB-R7943 decreased PVA without measurably changing Ca^{2+} decay kinetics, consistent with previous reports at similar doses.[9] Further, perfusion of KB-R7943 resulted in Ca_D elevation as described previously.[22] However, the greater contribution of SERCA2a to Ca^{2+} removal relative to NCX[23] may explain the less profound impact of partial NCX blockade on cytosolic Ca^{2+} accumulation compared with SERCA2a inhibition. Importantly, PVA is high in regions with relatively high NCX and low SERCA2a expression, or when SERCA2a is pharmacologically inhibited. These findings are consistent with previous reports of the anti-arrhythmic effect of NCX blockade in various models of long QT syndromes as well as during Ca^{2+} overload induced by cardiac glycosides.[8,9,24]

Unfortunately, whole-heart preparations and gross quantification of regional protein expression can only offer indirect evidence of the NCX to SERCA2a ratio. Future studies in isolated cardiomyocytes are necessary to determine whether NCX/SERCA2a is a determinant of arrhythmia propensity.

4.5 Mechanisms of PVA in DI-ATS1

It has been previously demonstrated that NCX is important for modulating SR Ca^{2+} release and itself can trigger SR Ca^{2+} release and thereby PVA.[25,26] Although this hypothesis has been controversial,[23] a mathematical model of increased $[Na^+]_i$ shifts the NCX current upwards.[27] A simulation in Supplementary material online, *Figure S3A*, demonstrates that either increasing $[Na^+]_i$ or $[Ca^{2+}]_o$ decreases the time to NCX reversal (Ca^{2+}-in–Na^+-out) during diastole. It is therefore possible that this diastolic NCX current reversal could trigger SR calcium release and the PVA observed in this model. Interestingly, late Na^+ current increases in response to elevated Ca_D,[28] and cardiac sodium channel (Nav1.5) expression is greatest in guinea pig LV.[11] Furthermore, preferentially reducing NCX

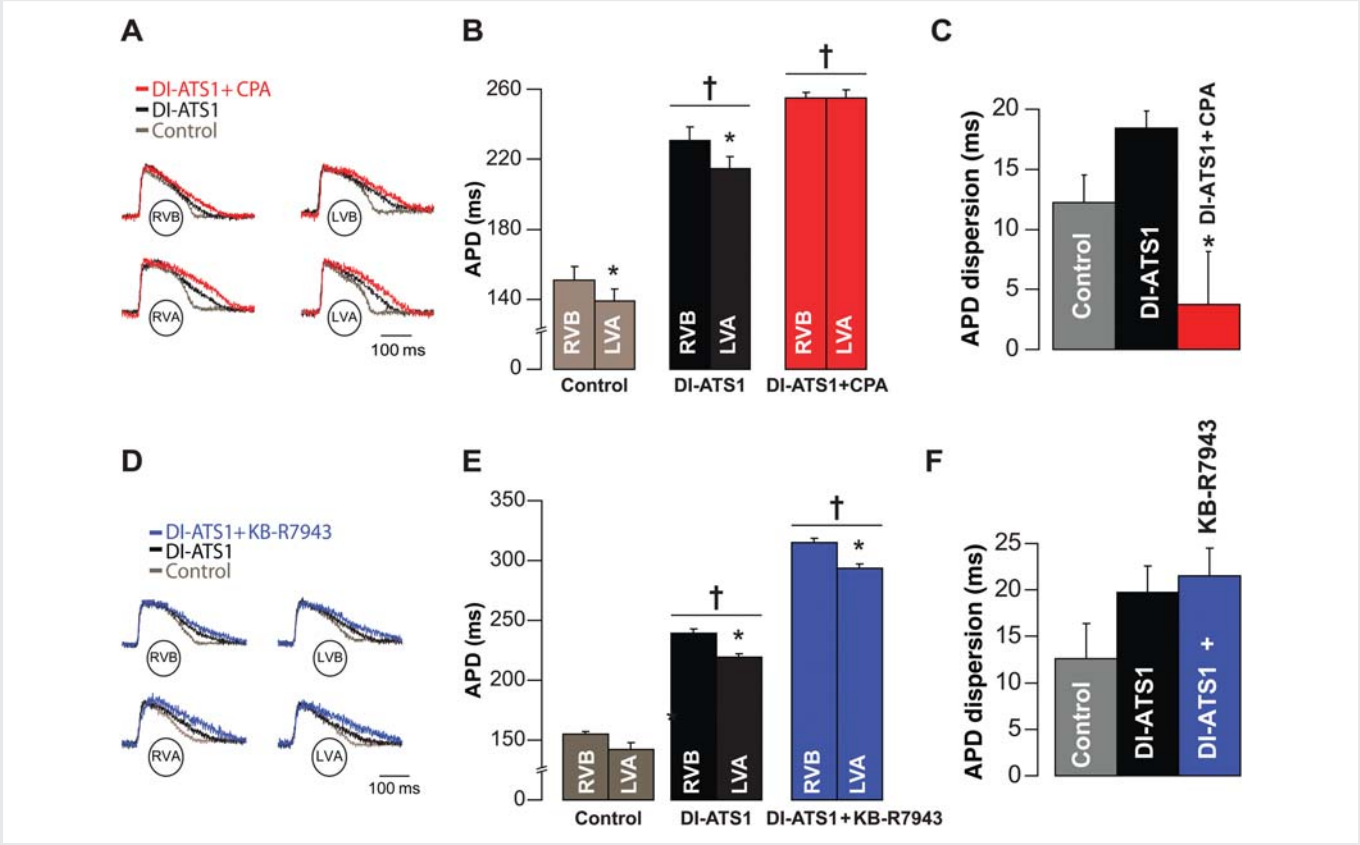

Figure 6 APD prolongation during pharmacological perturbations of DI-ATS1. (*A*) Representative optical action potentials recorded from same ventricular regions during control (grey traces) DI-ATS1 (black traces) and DI-ATS1 + CPA (red traces). DI-ATS1 prolonged APD relative to control. APD was further prolonged by DI-ATS1 + CPA. (*B*) The mean APDs demonstrate a rise in APD during DI-ATS1 compared with control ($^{\dagger}P < 0.05$, $n = 4$) that was further enhanced by DI-ATS1 + CPA ($^{\dagger}P < 0.05$ compared with DI-ATS1, $n = 7$). RVB–LVB APD difference during control ($^{*}P < 0.05$, $n = 4$) was maintained during DI-ATS1 alone ($^{*}P < 0.05$, $n = 7$). This was abolished during DI-ATS1 + CPA (P = NS, $n = 7$). (*C*) Total APD dispersion was reduced by DI-ATS1 + CPA relative to DI-ATS1 alone ($^{*}P < 0.05$, $n = 7$). (*D*) Representative optical action potentials recorded from the same ventricular regions during control (grey transients) DI-ATS1 (black traces) and DI-ATS1 + KB-R7943 (blue traces). DI-ATS1 + KB-R7943 prolonged APD and enhanced total APD dispersion. (*E*) The mean APD increased during DI-ATS1 + KB-R7943 compared with DI-ATS1 alone ($^{\dagger}P < 0.05$, $n = 7$) where the difference in APD between RVB and LVA was maintained ($^{*}P < 0.05$, $n = 7$). (*F*) Total APD dispersion was unaltered by DI-ATS1 + KB-R7943 relative to DI-ATS1 alone (P = NS, $n = 7$).

reverse mode, as is suggested action of KB-R7943,[9] reduces arrhythmia propensity. Taken together, these data support a hypothesis that enhanced PVA during DI-ATS1 is linked to reverse-mode NCX. However, isolated myocyte studies are needed to resolve this mechanism.

In summary, we present evidence that both an increase in Ca_D and high NCX expression are markers for the frequency and timing of PVA, and partially inhibiting NCX appears to be acutely anti-arrhythmic. Importantly, Ca^{2+} cycling is a complex process, since cytosolic Ca^{2+} is modulated by the myriad Ca^{2+} and Na^{+} handling proteins which may also be heterogeneously distributed throughout the heart.[11,18] Therefore, further studies are required to determine the effect of perturbation of Ca^{2+} and Na^{+} handling on the arrhythmia mechanisms outlined above.

4.6 Limitations

PVA is a relatively rare event in this model of DI-ATS1. Furthermore, transmural recordings demonstrate that the first beat can arise from any depth of tissue. Thus, it is likely that the actual site of triggered beat has not been fully mapped in this study particularly with respect to the optical mapping. We never recorded either the characteristic double Ca^{2+} transient related to triggered activity, or a gradual rise in membrane voltage as might be related to automaticity. Thus, we cannot exclude the possibility that PVA in this model is caused by spontaneous Ca^{2+} release or automaticity linked to NCX membrane depolarization. Further, protein expression does not necessarily correlate with protein function; therefore, future studies are needed to understand functional protein expression within each region of the myocardium.

Supplementary material

Supplementary material is available at *Cardiovascular Research* online.

Acknowledgements

We thank Alicja Booth for the preparation of the needle electrode and Wilson Lobaina for his generous assistance with needle electrode data acquisition.

Conflict of interest: none declared.

Funding

This research was supported by Nora Eccles Treadwell Foundation (to S.P.).

References

1. Tristani-Firouzi M, Jensen JL, Donaldson MR, Sansone V, Meola G, Hahn A *et al*. Functional and clinical characterization of KCNJ2 mutations associated with LQT7 (Andersen syndrome). *J Clin Invest* 2002;**110**:381–388.
2. Morita H, Zipes DP, Morita ST, Wu J. Mechanism of U wave and polymorphic ventricular tachycardia in a canine tissue model of Andersen–Tawil syndrome. *Cardiovasc Res* 2007;**75**:510–518.
3. Egdell RM, De Souza AI, Macleod KT. Relative importance of SR load and cytoplasmic calcium concentration in the genesis of aftercontractions in cardiac myocytes. *Cardiovasc Res* 2000;**47**:769–777.
4. Lukyanenko V, Subramanian S, Györke I, Wiesner TF, Györke S. The role of luminal Ca^{2+} in the generation of Ca^{2+} waves in rat ventricular myocytes. *J Physiol* 1999;**518**:173–186.
5. Diaz ME, Trafford AW, O'Neill SC, Eisner DA. Measurement of sarcoplasmic reticulum Ca^{2+} content and sarcolemmal Ca^{2+} fluxes in isolated rat ventricular myocytes during spontaneous Ca^{2+} release. *J Physiol* 1997;**501**:3–16.
6. Katra RP, Laurita KR. Cellular mechanism of calcium-mediated triggered activity in the heart. *Circ Res* 2005;**96**:535–542.
7. Radwański PB, Veeraraghavan R, Poelzing S. Cytosolic calcium accumulation and delayed repolarization associated with ventricular arrhythmias in guinea pig model of Andersen–Tawil syndrome. *Heart Rhythm* 2010;**7**:1428–1435.
8. Watano T, Harada Y, Harada K, Nishimura N. Effect of Na^+/Ca^{2+} exchange inhibitor, KB-R7943 on ouabain-induced arrhythmias in guinea-pigs. *Br J Pharmacol* 1999;**127**:1846–1850.
9. Satoh H, Ginsburg KS, Qing K, Terada H, Hayashi H, Bers DM. KB-R7943 block of Ca^{2+} influx via Na^+/Ca^{2+} exchange does not alter twitches or glycoside inotropy but prevents Ca^{2+} overload in rat ventricular myocytes. *Circulation* 2000;**101**:1441–1446.
10. Szentesi P, Pignier C, Egger M, Kranias EG, Niggli E. Sarcoplasmic reticulum Ca^{2+} refilling controls recovery from Ca^{2+}-induced Ca^{2+} release refractoriness in heart muscle. *Circ Res* 2004;**95**:807–813.
11. Veeraraghavan R, Poelzing S. Mechanisms underlying increased right ventricular conduction sensitivity to flecainide challenge. *Cardiovasc Res* 2008;**77**:749–756.
12. Haws CW, Lux RL. Correlation between in vivo transmembrane action potential durations and activation-recovery intervals from electrograms. Effects of interventions that alter repolarization time. *Circulation* 1990;**81**:281–288.
13. Poelzing S, Veeraraghavan R. Heterogeneous ventricular chamber response to hypokalemia and inward rectifier potassium channel blockade underlies bifurcated T wave in guinea pig. *Am J Physiol Heart Circ Physiol* 2007;**292**:H3043–H3051.
14. Restivo M, Caref EB, Kozhevnikov DO, El-Sherif N. Spatial dispersion of repolarization is a key factor in the arrhythmogenicity of long QT syndrome. *J Cardiovasc Electrophysiol* 2004;**15**:323–331.
15. Wei J, Liu H, Lee F, Lee M, Huang C, Pan H *et al*. Role of the sarcoplasmic reticulum in altered action potential and contraction of myopathic human and hamster ventricle. *Clin Exp Pharmacol Physiol* 2003;**30**:232–241.
16. Morita N, Sovari AA, Xie Y, Fishbein MC, Mandel WJ, Garfinkel A *et al*. Increased susceptibility of aged hearts to ventricular fibrillation during oxidative stress. *Am J Physiol Heart Circ Physiol* 2009;**297**:H1594–H1605.
17. Fujiwara K, Tanaka H, Mani H, Nakagami T, Takamatsu T. Burst emergence of intracellular Ca^{2+} waves evokes arrhythmogenic oscillatory depolarization via the Na^+–Ca^{2+} exchanger: simultaneous confocal recording of membrane potential and intracellular Ca^{2+} in the heart. *Circ Res* 2008;**103**:509–518.
18. Sims C, Reisenweber S, Viswanathan PC, Choi B, Walker WH, Salama G. Sex, age, and regional differences in L-type calcium current are important determinants of arrhythmia phenotype in rabbit hearts with drug-induced long QT type 2. *Circ Res* 2008;**102**:e86–e100.
19. Tweedie D, Harding SE, MacLeod KT. Sarcoplasmic reticulum Ca content, sarcolemmal Ca influx and the genesis of arrhythmias in isolated guinea-pig cardiomyocytes. *J Mol Cell Cardiol* 2000;**32**:261–272.
20. Abe F, Karaki H, Endoh M. Effects of cyclopiazonic acid and ryanodine on cytosolic calcium and contraction in vascular smooth muscle. *Br J Pharmacol* 1996;**118**:1711–1716.
21. Laurita KR, Katra R, Wible B, Wan X, Koo MH. Transmural heterogeneity of calcium handling in canine. *Circ Res* 2003;**92**:668–675.
22. Iwamoto T, Watano T, Shigekawa M. A novel isothiourea derivative selectively inhibits the reverse mode of Na^+/Ca^{2+} exchange in cells expressing NCX1. *J Biol Chem* 1996;**271**:22391–22397.
23. Sipido KR, Carmeliet E, Pappano A. Na^+ current and Ca^{2+} release from the sarcoplasmic reticulum during action potentials in guinea-pig ventricular myocytes. *J Physiol* 1995;**489**:1–17.
24. Milberg P, Pott C, Fink M, Frommeyer G, Matsuda T, Baba A *et al*. Inhibition of the Na^+/Ca^{2+} exchanger suppresses torsades de pointes in an intact heart model of long QT syndrome-2 and long QT syndrome-3. *Heart Rhythm* 2008;**5**:1444–1452.
25. Lipp P, Niggli E. Sodium current-induced calcium signals in isolated guinea-pig ventricular myocytes. *J Physiol* 1994;**474**:439–446.
26. Larbig R, Torres N, Bridge JHB, Goldhaber JI, Philipson KD. Activation of reverse Na^+–Ca^{2+} exchange by the Na^+ current augments the cardiac Ca^{2+} transient: evidence from NCX knockout mice. *J Physiol* 2010;**588**:3267–3276.
27. Armoundas AA, Hobai IA, Tomaselli GF, Winslow RL, O'Rourke B. Role of sodium–calcium exchanger in modulating the action potential of ventricular myocytes from normal and failing hearts. *Circ Res* 2003;**93**:46–53.
28. Maltsev VA, Reznikov V, Undrovinas NA, Sabbah NH, Undrovinas A. Modulation of late sodium current by Ca^{2+}, calmodulin, and CaMKII in normal and failing dog cardiomyocytes: similarities and differences. *Am J Physiol Heart Circ Physiol* 2008;**294**:H1597–H1608.